Investigation of Interactions between Mechanical and Electrical Components of a Motion Platform

Evrim Onur Ari
Unmanned Systems Department
ASELSAN Inc. Defense Systems Division
Ankara - Turkey
oari@aselsan.com.tr

Erol Kocaoglan
Department of Electrical and Electronics Engineering
Middle East Technical University
Ankara - Turkey
erolkoc@metu.edu.tr

***Abstract*—While modelling control systems with mechanical components driven by electrical motors it is usually assumed that the torque generating (electrical) sub-system has negligible dynamics and remaining study is based on this assumption. This paper is focused on investigation of the validity of this assumption. For this purpose, the interactions between mechanical and electrical components of a system consisting of an electrical motor connected to a mechanical load has been investigated by employing a simplified, linear model. Besides the analysis using this model, data collected via experiments on real hardware was processed and compared with the theoretical findings.**

I. Introduction

Motion platforms with payloads are widely used in modern defense systems (see Fig. 1). In most of these systems platform actuation is achieved by driving brushless electric motors via power electronic components (widely MOSFETs or IGBTs and their driver circuits). These components are controlled by processors which are capable of performing real-time calculations which use sensory information from gyroscopes, encoders, resolvers, inclinometers, force sensors, torque sensors etc. The aim of control during these calculations is generating "the correct motor current" which will move the platform with desired speed with respect to earth reference frame. Hence, the calculations try to suppress the disturbances (effects like hull motion, windage , sea waves etc.) while trying to obtain a closed loop transfer function from reference command to load speed equal to or at least very close to unity [5]. For this purpose, several techniques including resonance ratio control [1], model-predictive control (MPC) [12], robust control [7], resonant control [10], and techniques employing complicated sensor [8] and observer structures [11],[6],[2] are employed. During modelling and control phases, ,as also indicated by Szabat et. al. in their comparative study [9], most of these techniques assume that the motor current applied to the equivalent constant flux generalized machine's armature is proportional to the torque applied to the load and the dynamics governing the motor current is much faster than the dynamics of the mechanical system [3],[1]. However the interactions between mechanical and electrical components of the system might be a important factor and one should have an insight of these interactions while dealing with the controller design problem. In this study, we try to investigate the effects of mechanical system components on the control of motor current. Outline of the paper is as follows: In the second section, a simplified system model is analysed and its open- and closed-loop performances are investigated theoretically; in the third section, the analysis results are compared with the ones obtained experimentally on a sample system. The paper ends with a conclusion section.

Fig. 1. An example of a stabilized motion platform: Pedestal Mount Stinger Launching System - PMS ATILGAN® (Photo Courtesy of ASELSAN Inc.)

II. System Model

In the control of motion platforms usually flexible lumped mass mechanical models are employed. These models usually include two [3] or three [4],[11] lumped masses connected with flexible elements. For the control of flexible robot arms even four or more lumped mass models are employed [6]. For the purpose of investigating the interactions between mechanical and electrical components of such a flexible system, the model given in Fig. 2 is employed. The following assumptions are made in using this model:

- Dynamics of the drive electronics are neglected.
- Motor has been modelled as an equivalent permanent magnet DC motor with constant field flux. (generalized electrical machine model).
- Mechanical system is modelled as J_m representing motor and gearbox inertia;J_l representing load inertia;

978-1-4673-5769-2/13/$31.00 ©2013 IEEE

k_s and c_s representing stiffness and damping coefficients,respectively, of the connections between motor and load.

- Static frictions in the system are not modeled, and the only loss in the mechanical system is considered to be due to the c_s term.

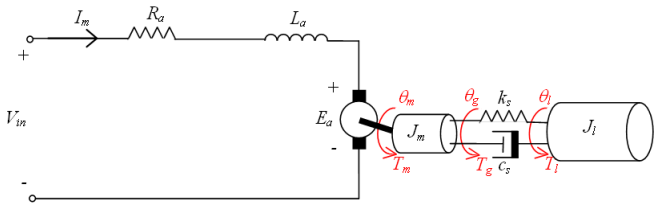

Fig. 2. Schematic representing the system model used for analysis.

A. Linear Analysis

The model shown in Fig. 2 consists of both electrical and mechanical components which are coupled via back-emf of the electrical motor. The parameters used in the model are summarized in Table I. We can write the voltage loop equation for the electrical part as follows:

$$V_{in} = R_a I_m + L_a \dot{I}_m + E_a \tag{1}$$

We can substitute the following equality instead of E_a in (1)

$$E_a = k_e \dot{\theta}_m n_g \tag{2}$$

by using standart motor model. Even if (2) seems to be a rather simple equation, it is the equation describing the physical phenomenon that interconnects the mechanical system with the electrical one. Since the model representing the motor inertia is free of stiffness and damping we can simply write

$$\theta_m = \theta_g \tag{3}$$

Using this assumption and Newton's 2^{nd} law of motion for the motor gives:

$$\ddot{\theta}_m = \frac{T_m + T_g}{J_m} \tag{4}$$

For the equivalent DC motors linearized torque equation we have

$$T_m = n_g k_t I_m \tag{5}$$

For the connection part, since it is inertia free we can write $-T_g = T_l$, which in turn yields

$$-T_g = T_l = k_s(\theta_m - \theta_l) + c_s(\dot{\theta}_m - \dot{\theta}_l) \tag{6}$$

Finally, applying Newton's 2^{nd} law of motion for the load inertia gives:

$$\ddot{\theta}_l = -\frac{T_g}{J_l} \tag{7}$$

Now,we will try to obtain the transfer function from input V_in to the output I_m using Laplace transforms of the previous time-domain equations

Taking Laplace transforms of (1) and (2), one gets

$$V_{in}(s) - (R_a + L_a s) I_m(s) - k_e n_g s \theta_m(s) = 0 \tag{8}$$

similarly, using (4) and (5), one gets

$$J_m s^2 \theta_m = n_g k_t I_m(s) - (k_s + c_s s)(\theta_m(s) - \theta_l(s)) \tag{9}$$

and lastly, using (6) and (7), one obtains

$$J_l s^2 \theta_l = (k_s + c_s s)(\theta_m(s) - \theta_l(s)) \tag{10}$$

Next, one can use (8),(9) and (10) to eliminate $\theta_l(S)$ and $\theta_m(s)$ and obtain

$$\frac{I_m(s)}{V_i n(s)} = \frac{s}{L_a s^2 + R_a s + k_e k_t n_g^2 \frac{J_l s^2 + c_s s + k_s}{J_l J_m s^2 + c_s (J_m + J_l) s + k_s (J_m + J_l)}} \tag{11}$$

Notice that equation (11) obtained above can be used to find the transfer function from V_{in} to I_m for the case in which motor is decoupled from the load (i.e. "Motor Only - MO" case) by setting $c_s = 0$, $J_l = 0$ and $k_s = 0$, yielding

$$\frac{I_m(s)}{V_i n(s)} = \frac{s}{L_a s^2 + R_a s + k_e k_t n_g^2 \frac{1}{J_m}} \tag{12}$$

B. Investigation of the Frequency Domain Behaviour

We now have the SISO system models for both "motor coupled to the load" (MCL) and "Motor Only" (MO) cases as transfer functions given in equations (11) and (12). In order to investigate the interactions between electrical and mechanical components we will compare these transfer functions. Moreover, we will extend this comparison into frequency domain in order to have a means of investigating the effects on a real system by means of frequency response tests.

In comparing these two transfer functions one must first note that they have very similar forms except the fact that the constant motor inertia term in equation (12) becomes a two-mass lumped mechanical system dynamics in (11) as expected. Another point which can be seen from the transfer functions is that the terms in denominators starting with $k_e k_t n_g^2$ couples the mechanical system to the electrical one, which is purely an $R-L$ circuit in the absence of this term. Hence this term is the one which transform the $R-L$ circuit into an electrical motor.

The frequency response functions (FRFs) corresponding to these transfer functions, obtained with the parameter values given in Table I are plotted in Fig. 3. As it can be seen in this figure, the two FRFs are quite different especially at low frequencies, for which motor "sees" both inertias for the MCL case. However at higher frequencies the two FRFs become very similar, as for the MCL case the motor and load inertias are decoupled due to slow mechanical dynamics of the mechanical interconnection and motor does not "see" the load inertia any more.

One of the most important information which can be obtained from FRFs are the resonance and anti-resonance frequencies, which also usually determine the performance of the closed-loop system since open-loop gain at the anti-resonance frequency is attenuated and the amount of gain at the resonance frequency usually determines the gain margin. The resonance frequency seen at the FRF of the MO case can

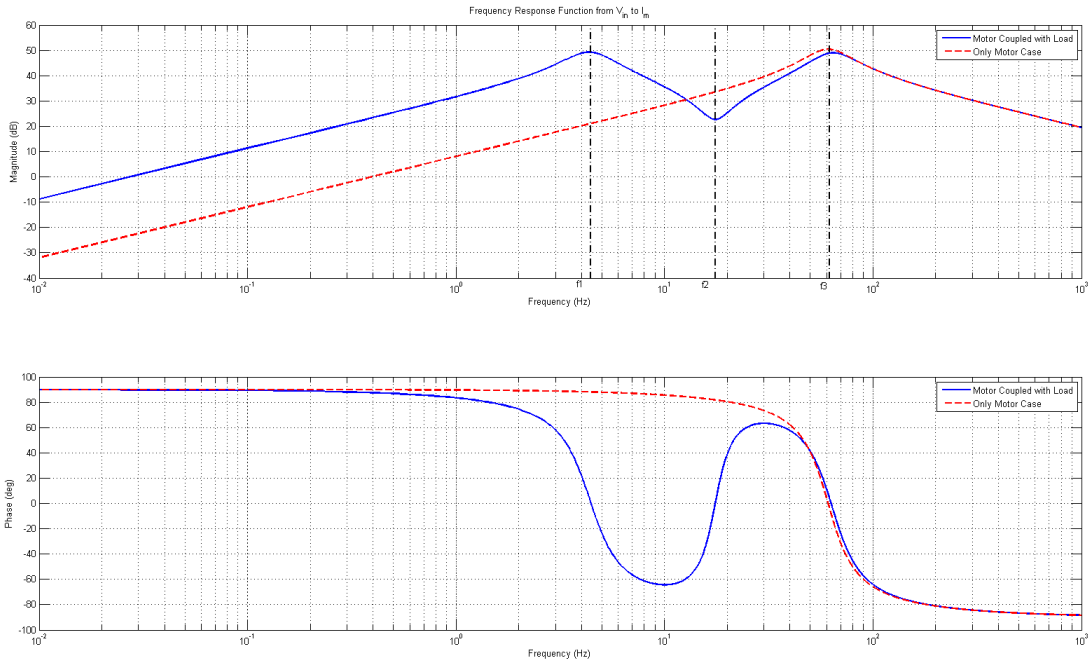

Fig. 3. Frequency response function plot of the SISO system models given in equations (11) and (12)

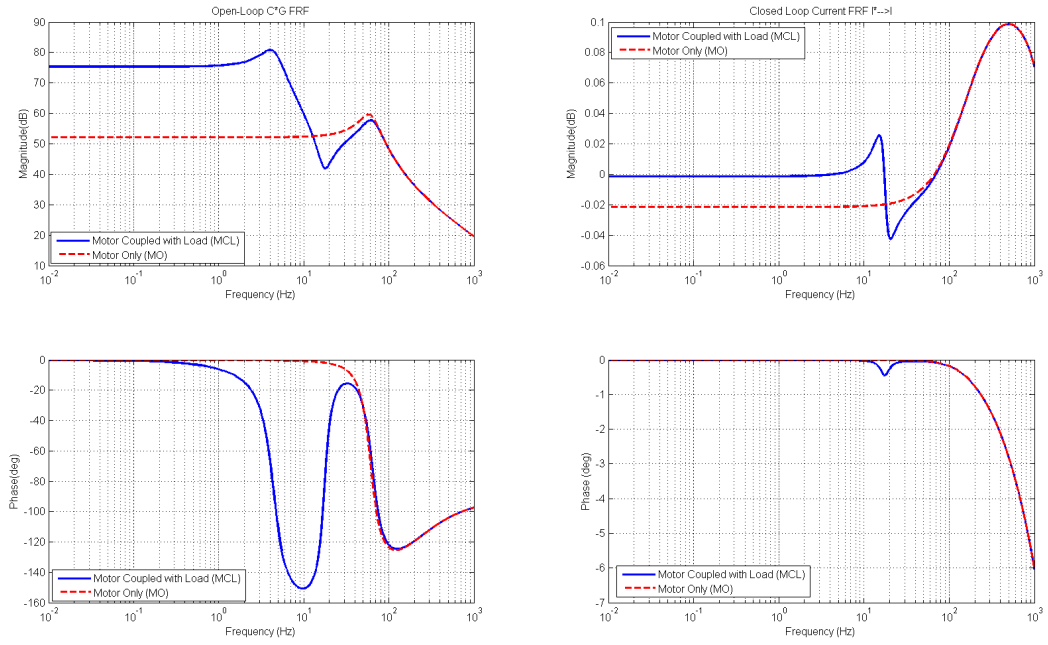

Fig. 4. Closed-loop frequency response function plot of the SISO system models given in equations (11) and (12) obtained with PI control with parameters $K_P = 1$ and $K_I = 1000$.

TABLE I. PARAMETERS OF THE SYSTEM MODEL GIVEN IN FIG. 2 AND SAMPLE VALUES USED DURING SIMULATIONS

PARAMETER	UNIT	REMARKS	SAMPLE VALUE
V_in	V	Terminal voltage of the equivalent permanent magnet DC motor.(applied by the motor driver)	Controlled
I_m	A	Armature current developed in the equavilent DC motor armature circuit.	Controlled
R_a	Ω	Armature resistance of the equivalent permanent magnet DC motor.	3 mΩ
L_a	H	Armature inductance of the equivalent permanent magnet DC motor.	17 mH
E_a	V	Back-emf voltage of the equivalent permanent magnet DC motor.	Controlled
T_m	Nm	Mechanical torque developed on motor shaft.	Controlled
θ_m	rad	Motor shaft position reflected to the load side.	Controlled
J_m	kgm^2	Equivalent load-side inertia of the motor shaft and gear box.	326 kgm^2
θ_g	rad	Gearbox output angular position.	Controlled
T_g	Nm	Torque at the gearbox output.	Controlled
θ_l	rad	Angular position of the Load	Controlled
c_s	Nm.s/rad	Equivalent damping coefficient for connections between motor and the load.	10 kNm.s/rad
k_s	Nm/rad	Equivalent stiffness coefficient for connections between the motor and the load.	3.675 Mnm/rad
J_l	kgm^2	Equivalent load inertia.	4400 kgm^2
k_e	V.s/rad	Back-emf constant of the equivalent DC motor.	0.125 V.s/rad
k_t	Nm/A	Torque constant of the equivalent DC motor.	0.125 Nm/A
I_m	A	Motor Armature Current	Controlled
n_g	$-$	Gear ratio of the gearbox (1:ng)	220

be approximately found by setting $R_a = 0$ in (12) and finding the denominator roots, which in turn yields:

$$f_3 = \frac{n_g}{2\pi}\sqrt{\frac{k_e k_t}{L_a J_m}} \tag{13}$$

This term is evidently a resonance arising from energy transfer between armature inductance and motor shaft inertia. Numerical value for f_3 for our system is found as 60.9 Hz which is also observed in the frequency response plot given in Fig. 3. In order to increase the resonance frequency for better control either the motor inertia and/or the motor winding inductance values should be decreased.

The anti-resonance frequency seen for the MCL case can be approximately found by setting $c_s = 0$ and finding the numerator roots of (11) ,the result is obtained as:

$$f_2 = \frac{1}{2\pi}\sqrt{\frac{k_s(J_m + J_l)}{J_m J_l}} \tag{14}$$

This value is exactly the same as the anti-resonance of the mechanical part of the system (starting with the motor shaft). As can be deduced from the form of the mechanical system, this anti-resonance is due to energy transfer between the combined inertia of the system and the stiffness of the connections, which is modelled as the spring k_s. f_2 is calculated as 17.5 Hz using (14) and this can be observed in Fig. 3.

The resonance frequencies seen in the MCL case can be approximately found by setting $c_s = 0$, $R_a = 0$ and solving for the roots of the denominator of (11) after setting $s = j\omega$, which yields the equation:

$$L_a J_l J_m \omega^4 - [k_s(j_m + J_l)L_a + J_l k_e k_t n_g^2]\omega^2 + k_s k_e k_t n_g^2 = 0 \tag{15}$$

with roots as shown in (16).

This result gives the first and second resonance frequencies for the MCL case as 4.43 Hz and 63.2 Hz which are also compatible with Fig. 3. Note that for the second resonance the energy transfer is mainly between the inductance and the motor inertia, while for the first resonance the effect would be more mechanical, as it is a rather low frequency resonance.

C. Closed-Loop System Performance

In the previous sub-section we have compared open-loop system characteristics for MCL and MO cases. In this sub-section we will compare the closed-loop performances.

As though the open-loop responses of the MO and MCL plants are quite different at low frequencies, while performing closed-loop control, controller transfer function also come into account. In this study, a classical PI controller is employed for both cases. In determining the controller parameters one can note that the transfer functions given in (11) and (12) both posses an open-loop zero at $s = 0$, hence both systems are natural "differentiators" up to a certain frequency. This can also be observed in the FRF given in Fig. 3. Hence, the integral part of the controller will effectively become a proportional controller. With high-enough K_I one can obtain the closed-loop frequency response performance shown in Fig. 4. In this figure, both the open-loop (including the controller) and closed-loop FRFs are given. In the open-loop FRFs it is seen that we have ∞ gain and phase margins for both systems although there is a collapse (due to resonance followed by an anti-resonance) in the phase for the MCL case. In the closed-loop FRFs it is seen that ,although the open-loop responses seem quite different, high open-loop gain suppresses this difference and makes the closed loop FRFs close to 1. Therefore, as a conclusion of the analysis we may state that with high-enough integral gain the current control performance for MCL and MO cases are indeed very similar.

III. PERFORMANCE OBTAINED WITH A REAL SYSTEM

In the previous section of the paper we have used a simplified model and shown that although open-loop system FRFs for MCL and MO cases are quite different, we can make both systems behave as unity gain closed loop systems for a high-enough frequency range by using a high K_I value in the controller. In this section, we will investigate the practical issues and try to infer any differences between the theoretical findings and actual system.

$$f_1, f_3 = \frac{1}{2\pi}\sqrt{\frac{1}{2}[\frac{k_s(J_m+J_l)}{J_m J_l} + \frac{k_e k_t n_g^2}{L_a J_m} \pm \frac{1}{L_a J_m J_l}\sqrt{J_l^2(k_s^2 L_a^2 + k_e^2 k_t^2 n_g^2 + 2k_s k_e k_t n_g^2 L_a) + J_m^2 k_s^2 L_a^2 + 2J_m J_l(k_s^2 L_a^2 - k_s k_e k_t n_g^2 L_a)}]} \tag{16}$$

We have performed open-loop frequency response tests with a motion control platform situated for control system design and testing. The parameters of this platform are given in Table I.The experimental open-loop response for the MO case is given in Fig. 5. If we compare the FRF given in this figure, with the one obtained from analysis (see Fig. 3) the following differences can be observed:

- Although the magnitude of the FRF follows a similar pattern with respect to frequency, the resonance is smoother, meaning that there exists further damping in the real system, which is possibly due to unmodeled rotor bearing friction.
- Phase of the FRF behaves differently than expected, and it is tending to be zero at very low frequencies. This means that the system actually has more damping terms than modeled making phase not equal to $90°$ as frequency is lowered. Moreover, due to fact that the resonance is smoother, the phase starts to decrease at a lower frequency, before the resonance peak.
- Phase of the FRF at high frequencies does not converge to the expected theoretical value. This fact indicates that there should be a transport delay term (with a transfer function $e^{-T_d s}$) causing more phase lag as the frequency is increased.

The experimental open-loop response for the MCL case is given in Fig. 6. If we compare the FRF given in this figure, with the one obtained from theoretical analysis (see Fig. 3) the following differences can be observed:

- Although the magnitude of the FRF follows a similar pattern with respect to frequency, both resonance peaks are smoother, meaning that there exists further damping in the real system, which is possibly due to unmodeled load and rotor bearing frictions.
- Phase of the FRF at high frequencies does not converge to a final value as expected from the analysis. This fact indicates that there is a transport delay term (with a transfer function $e^{-T_d s}$) injecting more phase lag as the frequency is increased.

The experimental closed loop responses for MO and MCL cases are given in Fig. 7 and Fig. 8, respectively. If one compares the magnitude plots given in these figures, it is seen that high integral gain suppresses the differences in the open-loop responses (though the resonances and anti-resonance of MCL case are still seen in the response, their magnitudes are quite small and phase jumps are eliminated). However, there is significant difference between expected and measured phase responses. As seen in Fig. 4 expected closed-loop phase lags are about $6°$ even at a frequency of 1 kHZ; however in the experiments it is seen that phase lag becomes about $80°$ even at 200 Hz for the MCL case. In order to find the reason for this difference a linear phase graph for the open loop motor only case is given in Fig. 9. in which the trend of phase difference between measured and expected phases is plotted. This phase scheme is very similar to the phase scheme of a transport delay which has a phase of

$$\theta = -T_d 2\pi f \tag{17}$$

where T_d represents the time delay in seconds. If we use origin and a point from Fig. 9 ($f = 66.5Hz$ and $\theta = -35.2° = 0.614rad$), we can find the delay amount as

$$T_d = -\frac{0.614}{2\pi 66.5} = 1.5ms \tag{18}$$

This very little amount of delay causes the closed loop current bandwidth of the system to degrade significantly. Hence, it is an important point to find the causes of this delay and try to minimize it.

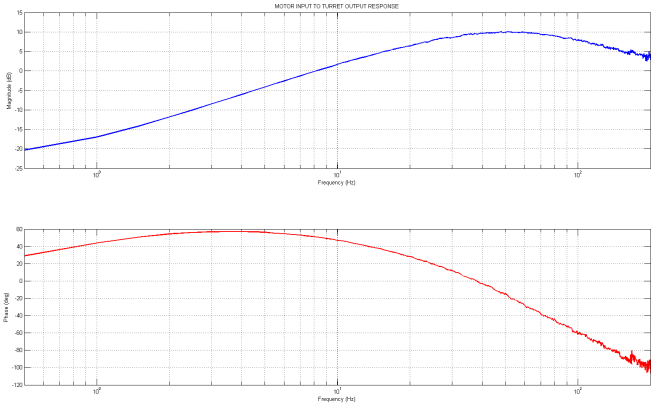

Fig. 5. Experimentally Obtained Open Loop System FRF for MO case

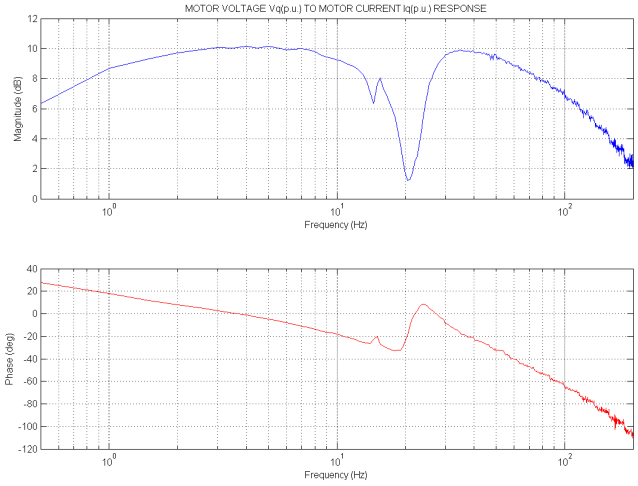

Fig. 6. Experimentally Obtained Open Loop System FRF for MCL case

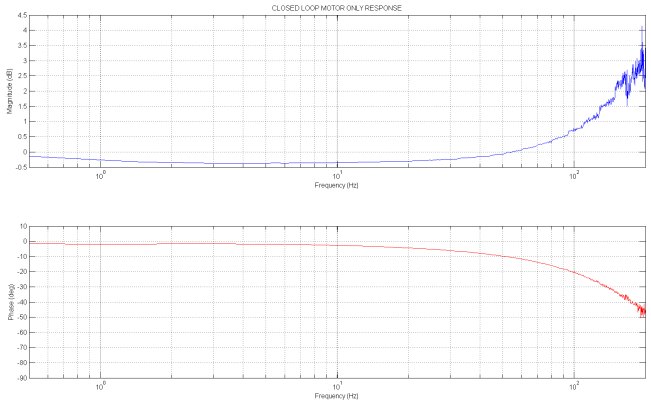

Fig. 7. Experimentally Obtained Closed Loop System FRF for MO case

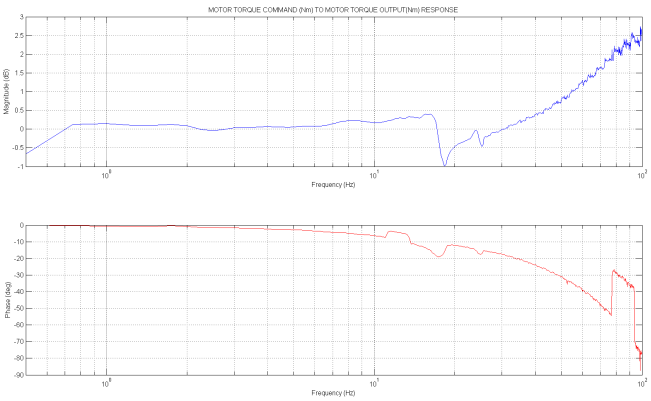

Fig. 8. Experimentally Obtained Closed Loop System FRF for MCL case

IV. Conclusion

The aim of this study was to explore the interactions between mechanical and electrical components of a motion platform. During the study both theoretical and experimental results are obtained and compared with each other. During theoretical calculations it was seen that when the motor is coupled to a load its open-loop transfer function from motor voltage to motor current is affected and FRF changes significantly. On the other hand, it was also shown that for a practical system (with high enough damping terms, i.e. electrical resistance and mechanical viscosity) this change can be suppressed via high enough integral control term while applying terminal voltage using motor current feedback during close-loop control. In this condition, the closed-loop motor current performance practically does not depend on whether the motor shaft is free to rotate or it is coupled to a mechanical load. This theoretical findings were observed during the experimental phase of the study as well. However, it was also observed that transport delays (mostly due to digital control and communications) affect the phase of the FRFs significantly, causing small gain margins and preventing an increase in integral gain and degrading closed-loop current performance significantly. This transport delay is usually the dominant factor in determining the bandwidth of the closed-loop current control and must be minimized with careful electronics and software design.

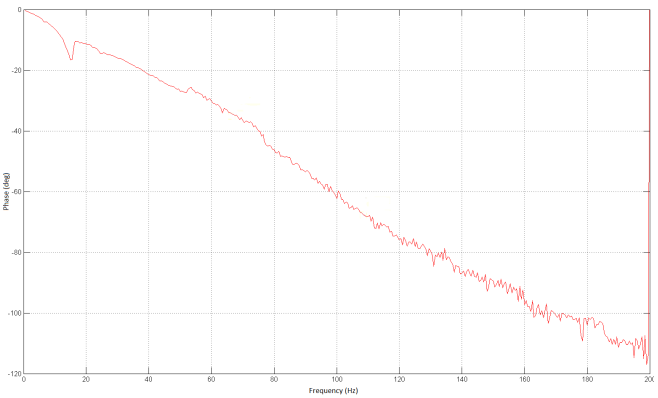

Fig. 9. Phase difference between theoretical and experimental MO FRF findings.(Note the linear trend indicating transport delay)

Acknowledgment

The authors would like to thank to Unmanned Systems Department at ASELSAN Inc. for both the experimental setups provided and the encouragement to perform this study as a part of professional work.

References

[1] Yuki K., Murakami T., Ohnishi K. Vibration Control of 2 Mass Resonant System by Resonance Ratio Control, *IECON'93 Proceedings*, Vol.3,pp 2009-2014,1993.

[2] Sugiura K., Hori Y. Vibration Suppression in 2- and 3-Mass System Based on the Feedback of Imperfect Derivative of the Estimated Torsional Torque, *IEEE Transactions on Industrial Electronics*, Vol. 43, No. 1,pp 56-64 ,February 1996.

[3] Zhang G., Furusho J. Speed Control of Two-Inertia System by PI/PID Control, *1999 International Conference on Power Electronics and Drive Systems*, pp 567-572, July 1999.

[4] Zhang G., Furusho J. Vibration Control of Three-Inertia System, *IECON'99 Proceedings*, Vol. 3,pp 1045-1050 ,1999.

[5] Ellis G., Lorenz R.D. Resonant Load Control Methods for Industrial Servo Drives, *IEEE Industry Applications Conference*, Vol.3, pp. 1438-1445, 2000.

[6] Hosaka M., Murakami T. Vibration Control of Flexible Arm by Multiple Observer Structure, *Electrical Engineering in Japan*, Vol. 154, No. 2, pp. 68-75, 2006.

[7] Xu Y., Wang X. Robust Vibration Control of Uncertain Flexible Structures with Poles Placement, *ISSCAA 2006 Proceedings*, pp 350-354 ,2006.

[8] OSullivan T.M., Bingham C.M., Schofield N. Observer-Based Tuning of Two-Inertia Servo-Drive Systems with Integrated SAW Torque Transducers, *IEEE Transactions on Industrial Electronics*, Vol. 54, No. 2, pp 1080-1091,April 2007.

[9] Szabat K., Orlowska-Kowalska T. Vibration Suppression in a Two-Mass Drive System Using PI Speed Controller and Additional Feedbacks - Comparative Study, *IEEE Transactions on Industrial Electronics*, Vol. 54, No. 2,pp 1193-1206 ,April 2007.

[10] Mahmood I.A., Moheimani R., Bhikkaji B. Precise Tip Positioning of a Flexible Manipulator Using Resonant Control, *IEEE/ASME Transactions on Mechatronics*, Vol. 13, No. 2, pp 180-186 ,April 2008.

[11] Celebi B. et. al. Motion Conrol and Vibration Suppression of Flexible Lumped Systems via Sensorless LQR Control, *Automatika*, Issue 51, pp 313-324, 2010.

[12] Cychowski M., Jaskiewicz R. Szabat K. Model Predictive Control of an Elastic Three-Mass Drive System with Torque Constraints, *ICIT 2010 Proceedings*, pp 379-385 ,2010.